

Manuscript title

Crystalline morphologies at the surface of PET/PEN random copolymer films

Abstract

A series of PET (poly(ethylene terephthalate)) / PEN (poly(ethylene 2,6-naphthalate)) copolyesters were synthesized by molten transesterification, and the surface crystallization behaviour of their thin films investigated by AFM with an *in-situ* heating stage. Force-distance measurements detected a surface glass transition (T_{gs}) of the copolymers several tens of degrees below their bulk glass transition (T_{gB}) obtained by DSC. The surface crystalline morphologies as a function of annealing temperature and film thickness were summarised as surface morphology diagrams. The surface crystallization temperature (T_{cs}) was found to be several degrees lower than the bulk crystallization (T_{cB}), and the films thinner than ~ 100 nm showed significant increase in T_{cB} . The lamellar crystalline morphology of copolymers with high randomness and short sequence length deviated from that of the homopolymers, reflecting the composition and degree of randomness. Highly random PET/PEN=75/25wt% copolymers exhibited unique lamellar curvature with arbitrary growth directions. Sharp boundaries between the crystals and amorphous suggested an absence of large amounts of rejected material at the growth front. In the case of copolymers with high randomness and short sequence length, no bulk crystallization morphology was observed even at 190°C, with the relatively thick surface crystalline layer totally covering the emergence of any bulk crystals.

Keywords

Surface glass transition, surface crystallization, thin films, copolymers, co-crystallization, morphology

Authors

Kei Shinotsuka and Hazel E. Assender*

Department of Materials, University of Oxford, Parks Road, Oxford, OX1 3PH, UK

1. Introduction

Crystallization in random copolymers will be influenced by the ability of random sequences of monomers to form ordered crystal structures. Thus, we would expect that the amount of crystallization, the crystallization temperature, and the crystal morphology will all be affected by the nature of the different comonomers, the relative proportions of the monomers, and the sequence (in particular the degree of ‘blockiness’/randomness) of the monomers. Many studies have been made of crystallization of polymers in thin films and at the surface of films, and copolymerization would be expected to have an influence on this behaviour. In observing the behaviour of copolymer crystallization we should draw upon the understanding of how random sequences of monomers may form regions of ordered, crystalline material. Flory [1] suggested that crystallization in a random copolymer system may take place based on matching of homopolymer sequences of the crystallizable component while the non-crystallizable component is rejected into the interlamellar amorphous regions. Later, kinetic constraints were introduced into Flory’s model [2], in which only the nearest neighbouring molecules are capable of adding to the crystal, and different units could be treated as defects in the crystal.

It has been experimentally demonstrated that there are some copolymers in which only one component is crystallizable and the other component is rejected from the crystal. For example, in the case of the random copolymer systems such as poly(butylene terephthalate) (PBT) / poly(tetramethylene ether glycol) [3], poly(butylene succinate) (PBS) / PBT [4], ethylene-octene olefin copolymers [5], and PET / poly(ethylene oxide) [6], the crystallization of two components occurs competitively resulting in mesophase separation, with the minor component rejected from the crystalline phase.

In contrast to this ‘rejection of the non-crystallizing component’ model, if the two crystallizable polymers have similar molecular structure, co-crystallization of the two components may take place. Random copolyesters of PET / PEN [7, 8], PET / poly(ethylene isophthalate) (PEI) [9], poly(trimethylene terephthalate) (PTT) / PEN [10], and PEN / poly(pentylene terephthalate) (PPT) [11] are known to show co-crystallization behaviour, in which both monomers are included in the crystals. Windle *et al.* [12, 13, 14, 15, 16] conducted diffraction studies of PET/PEN random copolymers, reporting that co-crystallization of terephthalate and naphthalate units is possible by lateral matching of similar monomer sequences. According to this idea, even the mixtures that contain different monomer units and lack periodicity in the chain direction are able to crystallize by sequence matching with neighbouring chains. It was found that a set of unit cell parameters of the random copolymer crystals changes gradually from one homopolymer to the other as a function of the PET/PEN composition [14]. Gutierrez *et al.* [17] also proposed a similar idea based on the XRD results of copolyesters prepared from 4-hydroxybenzoic acid and 2-hydroxy-6-naphthoic acid.

In this study, we consider three aspects of the crystallization behaviour. Firstly we present the surface glass transition temperature, T_{gs} , of a series of PET/PEN random copolymer films, which implies enhanced mobility at the surface and consider the thickness of the surface layer and surface crystals [18, 19] depending on the degree of randomness. Secondly, we map the surface morphology diagrams of the copolymer films as functions of film thickness and crystallization temperature, which indicate both characteristic surface crystallization behaviour and influences by degree of transesterification. Thirdly, as the surface crystallization gives rise to very clear morphologies that can be examined by AFM, we utilize this opportunity to examine lamellar

morphologies of the copolymer crystals which depend on the film thickness, and the composition and regularity of the copolymers, aiming to provide a better understanding of the crystallization of heterogeneous monomer units.

2. Experimental

2-1. Copolymer synthesis

This study is presented as a continuation of our previous work in which the synthesis and molecular characterization of a series of PET/PEN copolymers is reported in detail [20]. PET (Sigma Aldrich) and PEN (kindly provided from Teijin Chemical Co., Ltd) at various ratios were co-dissolved in a mixed solvent of 70 wt% 2-chlorophenol (Fisher Scientific) and 30 wt% 1,1,1,3,3,3-hexafluoro-2-propanol (Sigma Aldrich). Solutions were filtrated with 0.2 μm pore sized PTFE syringe filters (Gelman), and coprecipitated by pouring the solution into acetone [21]. The precipitation was thoroughly washed with acetone by Soxhlet extractor for 48 hours, and dried in a vacuum oven at 120 °C for 24 hours. From these mixed precipitates, a series of PET/PEN copolymers (Table 1) were synthesised by transesterification reaction for study in this work. Different mixing ratio and reaction periods were used to form the various copolymers of different composition and randomness. The transesterification reaction was carried out in the molten state in a differential scanning calorimeter (DSC) (Perkin Elmer DSC-7) [21] at 300 °C for 5, 20, and 60 minutes in an argon gas atmosphere. During transesterification, series of segments swap between one chain and another, and thus, as the reaction proceeds, the ‘runs’ of one monomer type that have not been transesterified with another chain decreases. Hence a longer reaction time leads to shorter sequence lengths of the same monomer, i.e. a more random chain.

The viscosity average molecular weights of the product copolymers were determined by Ubbelohde viscometry with application of the Mark-Houwink-Sakurada equation [22].

2-2. DSC

The bulk thermal behaviour of PET, PEN and their copolymers (as-synthesised material) was measured by DSC (Perkin Elmer DSC-7) at a heating rate of 10 °C/min in an argon gas atmosphere. DSC traces are presented in the Supporting Information section (Fig.S1).

2-3. ^1H NMR spectroscopy

The series of synthesized copolymers were dissolved in deuteride 1,1,1,3,3,3-hexafluoro-2-propanol (Sigma Aldrich) at 1.0 wt%, and ^1H NMR spectroscopy was carried out at 27 °C with high resolution 500 MHz NMR (Bruker DRX 500, TBI probe, 16 scans, recycle delay = 1.0 sec, acquisition time = 3.2 sec) to determine the statistical sequence length and the degree of randomness of the copolymers. The sequence length and degree of randomness of the copolymers were obtained by the following calculations [23], reported in our previous work [20] in detail.

$$L_T = 1 + 2A_{TET}/A_{TEN} \quad (1)$$

$$L_N = 1 + 2A_{NEN}/A_{TEN} \quad (2)$$

$$B = 1/L_T + 1/L_N \quad (3)$$

where L_T and L_N are the number average sequence length of ethylene terephthalate units and ethylene naphthalate units, and B is defined as degree of randomness, where $B = 0$ indicates all units the same (a homopolymer), $B = 1$ would be the case of a fully random distribution of units, and $B = 2$ would correspond to an alternating copolymer of the two monomers. A_{TET} , A_{TEN} , and

A_{NEN} are ^1H NMR peak areas of each of three independent resonances for NEN (4.879 ppm), TEN (4.828 ppm), and TET (4.776 ppm), where NEN indicates the ethylene groups between two naphthalene groups, TEN the ethylene groups between naphthalene and terephthalate groups, and TET the ethylene groups between two terephthalate groups.

2-4. *In-situ* AFM observation

Amorphous polymer films of various thicknesses were deposited on single crystal silicon substrates (Compart Technology, orientation (100) plane) by spin coating at 3000 rpm (solutions were filtrated with 0.2 μm pore sized filters beforehand), and dried in a vacuum oven at 40 °C for 6 hr. The film thicknesses were measured using an ellipsometer (Rudolph Research / Auto EL).

The developing crystalline morphology was observed at a range of temperatures, using an atomic force microscope (AFM) (Auto-probe CP microscope, Park Scientific Instruments) at a scanning rate of 0.5 Hz. Each sample cast on a Si substrate was set on a specially designed *in-situ* heating stage placed on an AFM scanner, and annealed at elevated temperatures ranging from 50 to 190°C. The heating was performed stepwise from low to high temperatures and samples were kept at each elevated temperature for two hours before the morphology was recorded. All the AFM data shown in this study are topographic images where whiter areas correspond to a higher surface. The characteristic morphologies of the surface (many examples of which are given in this manuscript e.g. Figs. 2 & 4) and bulk crystallinity (an example of which is given in Fig. S2 in Supplemental Information) can be used to determine whether surface or bulk crystallization has occurred at a specific annealing temperature in the thin films. A full description of this method is given in [24].

2-5. Force-distance curve analysis

Scanning force microscope (SFM) force-distance curve measurements of polyesters and copolyesters were carried out using the same AFM used for the morphology study. Details of the measurements and an example analysis are described in the Supporting Information section (Fig.S3). The spin-coated films were attached on the *in-situ* heating stage and force-distance curve measurements were taken with the same V-shaped cantilever as the topographic images (contact force of 0.24 nN, contact frequency of 0.7 Hz). The force-distance behaviour from AFM curves has been used by multiple groups for the determination of a change in properties, associated with T_g [18, 24, 25, 26, 27, 28]. For measurements reported here, the T_g at the near surface was determined from the observed change in the snap-off displacement vs. temperature, [18, 24, 25]. The snap-off displacement at each temperature was taken as the mean of 30 measurements from different locations on the sample. Example data are shown in Supporting Information (Fig.S3)

3. Results and Discussion

3-1. Molecular weight, sequence length, and degree of randomness

The molecular weight, sequence length, and degree of randomness of synthesized PET/PEN copolymers are summarized in Table 1. The measured molecular weights are thought to be large enough to exemplify polymeric behaviour of the products. As the reaction progresses, the sequence length L_T and L_N gradually decreases and degree of randomness B increases, depending on the ester exchange reaction rate. The observed behaviour of the sequence length and the degree of randomness are consistent with previous reports of the copolymerization of PET/PEN [29-34].

Table 1 Synthesized PET/PEN copolymers

	Composition	Reaction time	Molecular weight	Sequence length		Degree of randomness
	PET/PEN	min	kDa	L_T	L_N	B
PET	100/0	0	25.9	homopolymer		0.00
Copoly 6	90/10	5	13.4	400	23	0.05
Copoly 4	90/10	60	13.0	12	1.2	0.95
Copoly 10	75/25	60	12.3	5.1	1.2	1.00
Copoly 3	50/50	5	12.8	29	25	0.08
Copoly 1	50/50	60	14.9	2.1	1.7	1.06
Copoly 13	25/75	60	16.4	1.5	4.4	0.91
Copoly 7	10/90	60	12.2	1.1	20	0.97
Copoly 9	10/90	5	12.9	21	280	0.05
PEN	0/100	0	14.5	homopolymer		0.00

Reaction temperature: 300°C

3-2. Bulk and surface thermal transition temperatures

T_{gS} of each of the copolymers was determined by analysing their SFM force distance curve at elevated temperatures. Previous analysis of both PET and PEN [24] indicated that T_{gS} is constant with film thickness. Under cold crystallization we would expect the onset of crystallization to occur above the glass transition temperature, so we would expect that the surface crystallization temperature, T_{cS} , and bulk crystallization temperature, T_{cB} would occur above the respective glass transitions: T_{gS} and the bulk glass transition temperature, T_{gB} . Table 2 shows T_{gS} of the copolymer films determined by SFM force distance curve compared with T_{cS} by AFM, and T_{gB} and T_{cB} , by DSC. All the T_{gS} of the copolymers are smaller than their T_{gB} , suggesting the existence of surface layer near the polymer-air interface wherein enhanced polymer chain mobility is manifest in reduced glass transition temperatures [18, 24-28, 35-38]. Copolymers close the central compositions e.g. 10, 3, 1, and 13 exhibited T_{gS} closer to the T_{gB} for the same copolymers.

Table 2 Summary of thermal transition temperatures for PET/PEN copolymers

	Composition	Reaction time	T_{gs} by FD curve	T_{cs} by AFM	T_{gb} by DSC	T_{cb} by DSC
	PET/PEN	min	°C	°C	°C	°C
PET	100/0	0	48.1	70	71.1	130.0
Copoly 6	90/10	5	48.7	70	77.8	140.9
Copoly 4	90/10	60	47.0	70	72.9	137.6
Copoly 10	75/25	60	71.9	95	80.4	176.9
Copoly 3	50/50	5	74.7	90	87.3	182.8
Copoly 1	50/50	60	79.5	-	88.9	-
Copoly 13	25/75	60	102.2	135	105.0	-
Copoly 7	10/90	60	86.5	115	108.3	191.5
Copoly 9	10/90	5	78.4	100	108.1	177.9
PEN	0/100	0	85.4	115	112.0	201.0

The data for T_{cs} (surface crystallization temperature) are for the thick films.

The data for T_{cb} (bulk crystallization temperature) are the maxima of the exotherm by DSC, hence onset temperatures are lower.

DSC traces are presented in supporting information (Figure S1), from which T_{cb} and T_{gb} (bulk crystallization and glass transition temperatures respectively) are determined.

T_{gs} (surface glass transition temperature) is determined from AFM force-distance curves.

3-3. Surface morphology diagrams and trends in morphology

In this section we consider groups of copolymers (PET-rich, PEN-rich and the 50:50 mixtures) in turn and examine the morphological variations seen with composition and with different degrees of randomness (transesterification time). The morphologies observed at the surface are summarised in surface morphology diagrams that give an overall ‘map’ of the crystallization behaviours as a function of films’ thickness and annealing temperature.

Although we cannot dismiss the possibility that there is some preferential surface segregation of different components, meaning that the surface region might have a different molecular weight and/or composition than the average of the whole sample, the trends observed strongly suggest that this is not a dominant effect (e.g. composition segregation would serve to suppress changes observed as a function of composition), and for the purposes of this discussion we have assumed that there is no significant surface segregation.

PET-rich copolymers

The surface morphology of thin films of PET and PET-rich copolymers, as observed from the AFM imaging, as a function of annealing temperature are summarized as the surface morphology diagrams in Fig.1. Indices in the diagrams correspond with the example AFM images in Fig.2.

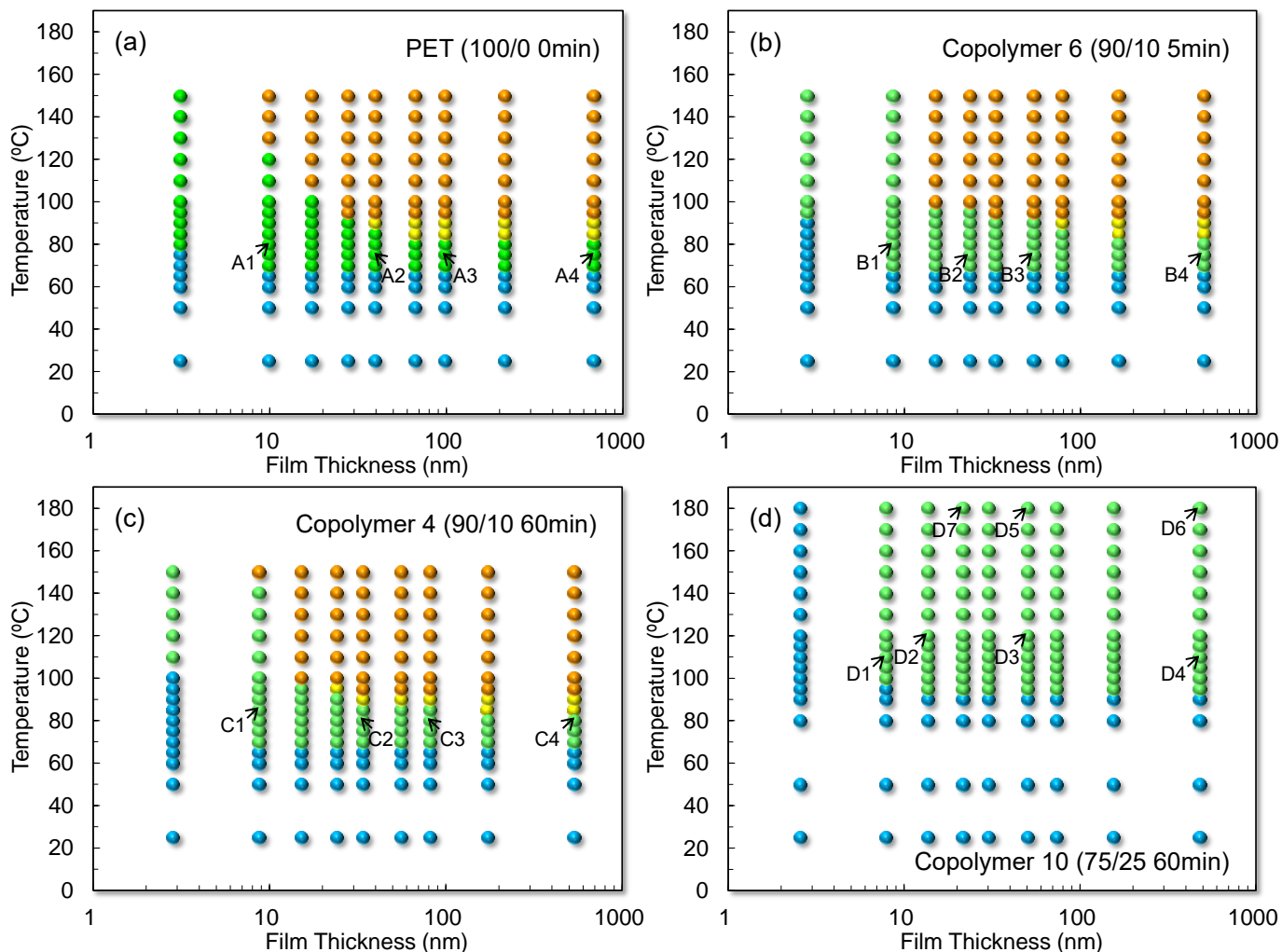


Fig.1 (Colour online) Surface morphology diagrams of PET and PET-rich copolymer thin films (percentage PET and reaction time is given for each case). Surface morphology of the thin films were recorded after a 2-hour annealing at each temperature in increasing steps. Blue: amorphous, Green: surface crystals, Orange: bulk crystalline. Yellow represents an intermediate structure in which the surface crystalline morphology has not been fully broken up by the emergence of bulk crystallites. The labelled points (A1-D7) indicate the conditions corresponding to the AFM images shown in subsequent figures.

Fig.1-a represents the surface morphology diagram of homopolymer PET. As thick films are annealed at increasing temperatures, the originally amorphous, featureless, surface firstly produces surface crystals (e.g. at 70°C, see Fig 2, A4). These surface crystals are thought to emerge and develop within the limited-depth surface layer where the more mobile material occurs due to the lower T_g at the surface: an Avrami macro kinetic analysis concluded their crystal dimension is two-dimensional [18]. Subsequently, as the film is annealed at temperatures higher than T_{CB} , the characteristic surface crystalline morphology is no longer observed, but is replaced by the, much rougher, characteristic bulk crystalline morphology (Fig. S2). The surface crystals are thought to be broken (or obscured by the, now much rougher, surface) or reintegrated (by an Ostwald ripening-type of process) by the forming bulk crystals once the bulk polymer beneath the surface layer becomes mobile. The surface crystalline region is shown in Fig.1-a to have a 15°C temperature range in between the amorphous and bulk crystalline regions. If the film thickness is smaller than ca.70 nm, morphological T_{CB} is greatly increased. Images from A1 to A4 in Fig.1-a

show the thickness dependence of the crystalline morphology of PET thin films. The details of the

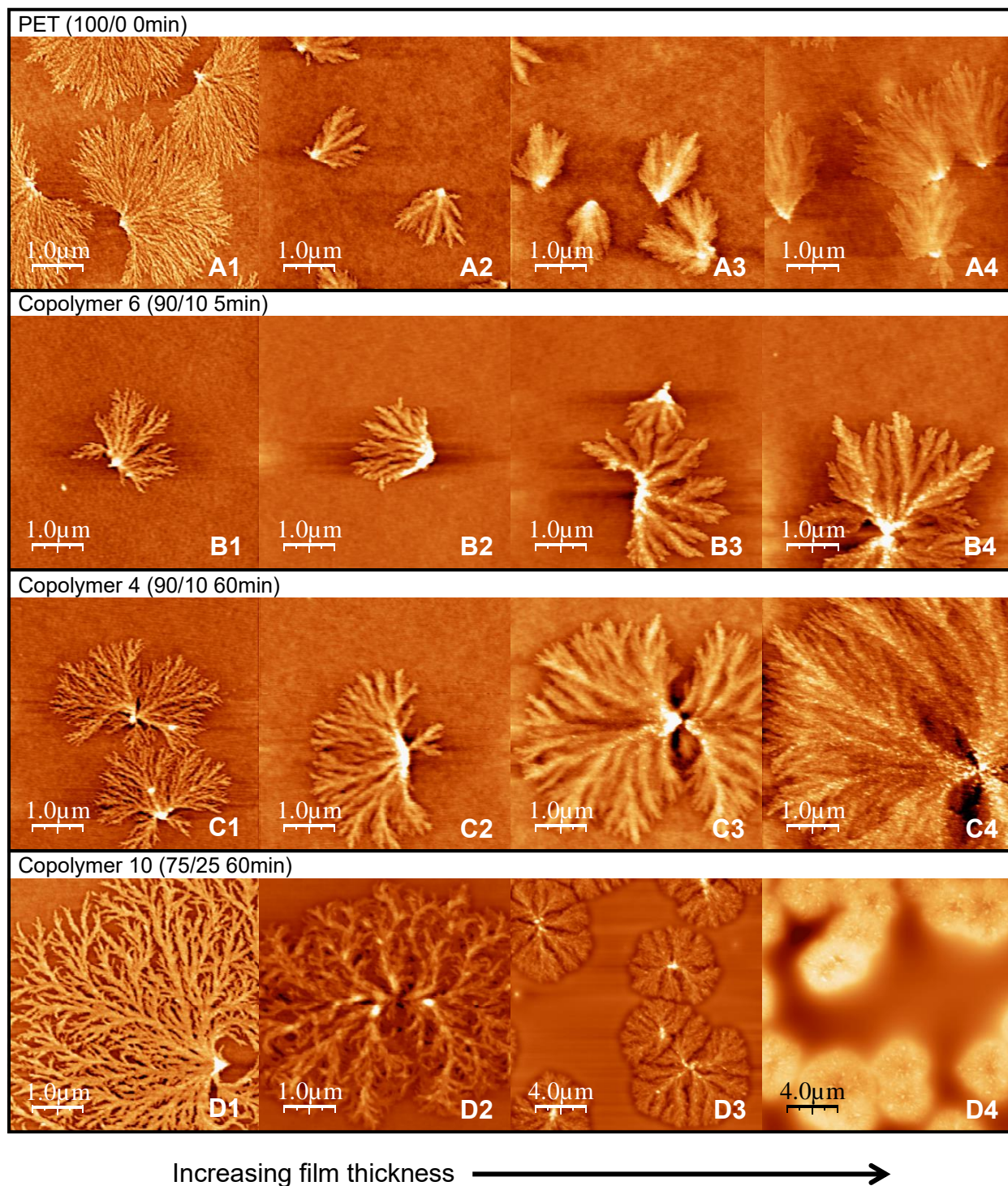


Fig.2 (Colour online) Surface crystals of PET and PET-rich copolymers corresponding to the crystal stability diagrams in Fig.1. Images from A1 to A4 are PET (thicknesses 10, 40, 100 and 700 nm), B1 to B4 are Copolymer 6 (PET/PEN=90/10, 5 min reaction, thicknesses 9, 25, 50 and 500 nm), C1 to C4 are Copolymer 4 (PET/PEN=90/10, 60 min reaction, thicknesses 9, 32, 80 and 550 nm), and D1 to D4 are Copolymer 10 (PET/PEN=75/25, 60 min reaction, thicknesses 8, 15, 50 and 477 nm), respectively. Images left-to-right are from films of increasing thickness. The morphological feature of PET and PET-rich surface crystals in small thickness is to grow straight from the core, forming a fan-shape at first (images from A to C). In the case of Copolymer 10 (PET/PEN = 75/25), on the other hand, the morphology is dramatically changed, giving spherulitic surface crystals in thick films (D3 and D4), while fine branching in thin films (D1 and D2).

crystallization of PET films are reported in our previous works [18,24].

The crystallization behaviour of Copolymer 6 (PET/PEN = 90/10, 5 min reaction), Fig.1-b, is basically analogous to PET, although repression of bulk crystallization is still observed in layers that are slightly thicker, and the onset of surface crystallization in the thinnest films occurs at a higher temperature. Thus, crystallization of Copolymer 6 is deduced to be more difficult in very thin films (less than ca.10 nm), whereas thicker films exhibit similar behaviour to PET. The AFM images of surface crystals of Copolymer 6 are shown from B1 to B4 in Fig.2. These crystalline morphologies are strongly influenced by the major component, PET, resulting in the PET-like fan-shape crystals, although the frequency of branching seems to be slightly greater than that of homopolymer PET.

Copolymer 4 (PET/PEN = 90/10, 60 min reaction) showed similar propensity in crystalline morphology (Fig.2, C1 to C4) and a similar surface morphology diagram (Fig.1-c), although there is some increase in lamellar branching and emerging bristle-like protrusions on the lamellar surface in thick films (Fig.2, white spots on the surface crystals in C3 and C4).

In this range of PET/PEN composition (from 100/0 to 90/10), it seems that the copolymer would never lose crystallizability at any degree of transesterification, because the quantity of major component PET units is sufficient to overcome the existence of heterogeneous PEN units, by rejecting PEN units from the primary lamellae body, and/or skipping or including PEN units inside of lamellae as crystalline defects. The incorporation of PEN units might account for the increased branching in Copolymer 6 and Copolymer 4, as PEN has been shown to be more highly branched [24], but we cannot eliminate the possibility that a change in interfacial properties due rejection of PEN units onto the surface of the developing crystal might also encourage branching.

In the case of Copolymer 10 (PET/PEN = 75/25, 60 min reacted), which has a higher degree of randomness B (1.00) and shorter sequence length L_T (5.1) than Copolymer 4, it is expected that crystallization would be restricted to some extent, and indeed, Fig.1-d, T_{cS} was observed at 95°C, which is 25°C higher than that of PET. For this short sequence length material there was no bulk crystallization observed with the AFM, such that the surface crystalline morphology was sustained even until 180°C. The thinnest film (2.6 nm) did not show surface crystals even at 180°C. As shown in images from D1 to D4 in Fig.2, the crystalline morphology of Copolymer 10 is dramatically different from that of PET. In thick films such as D4 (477 nm), lumps of crystal developed with rather spherulitic appearance, whereas fine branches developed in the thinner films of D2 (30 nm) and D1 (7.8 nm). The branching frequency became even higher than Copolymer 6 and 4 (90/10 composition), forming a complex morphology distinct from that of PET. L_T of Copolymer 10 is less than half (5.1) that of Copolymer 4, while L_N is nearly the same (1.2). Because of the increased probability of the crystalizing chain next containing a heterogeneous PEN component, crystal formation involves a larger number of defects, resulting in plentiful anomalous branching and lamellar deformation.

PEN-rich copolymers

In many respects, the changes in behaviour at the PET-rich end are reflected at the PEN-rich end of the composition range. The surface morphology diagrams of PEN-rich copolymers are presented in Fig.3. Although the shape of the diagram seems similar to that of PET, the T_{cS} and T_{cB} of PEN diagram (Fig.3-a) are 45°C higher than that of PET and crystallization is repressed more in the thinnest films. Compared with PET, the primary morphological feature of PEN surface

crystals is fine and high-dense branching in all growth directions as shown in Fig.4-E1 to E4. In addition, if film thickness is larger than ca. 60 nm, fine bristle-like objects protrude vertically from the surface of the crystals (E3 and E4).

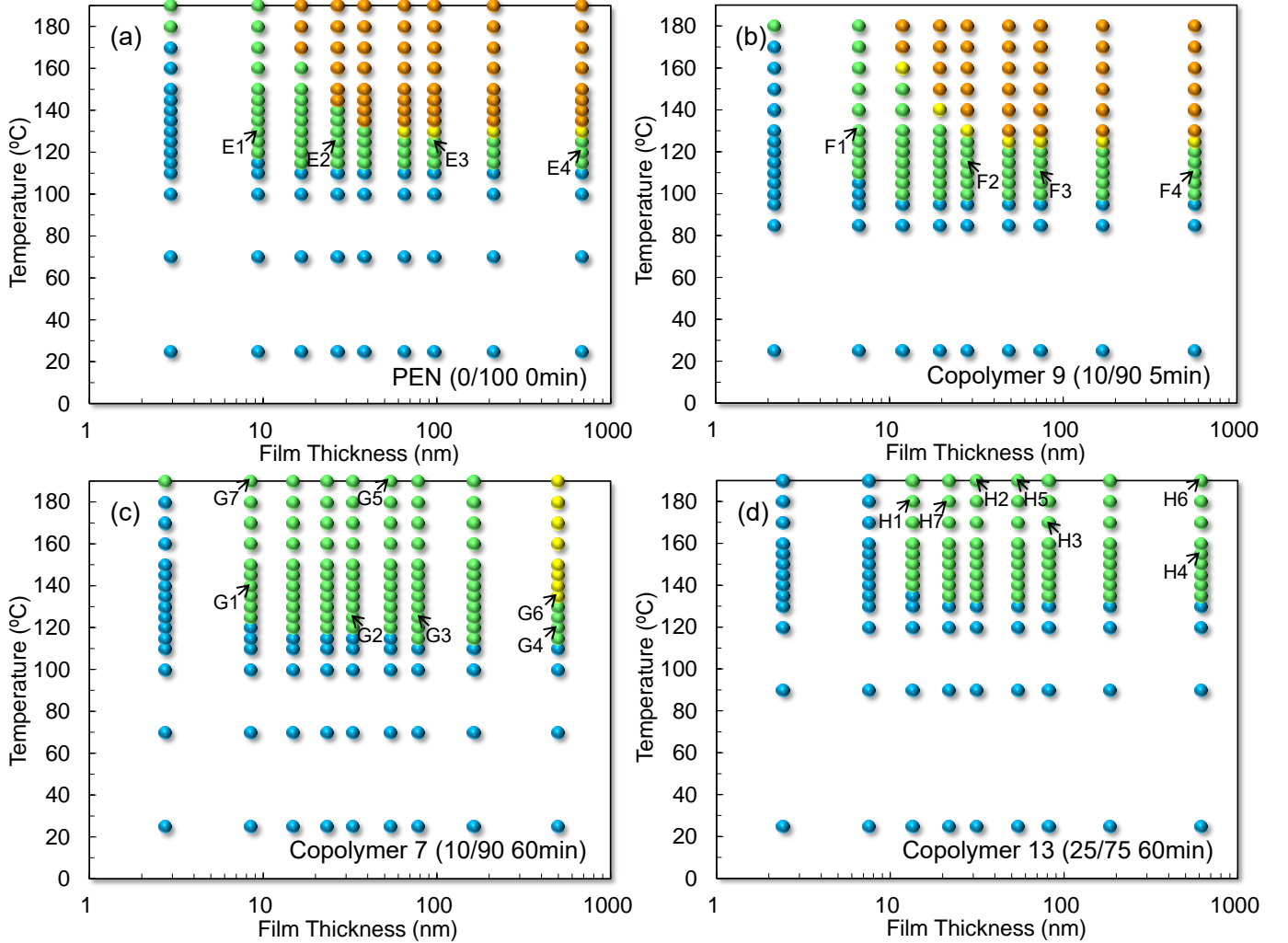


Fig.3 (Colour online) Surface morphology diagrams of PEN and PEN-rich copolymer thin films. Surface morphology of the thin films were recorded after a 2-hour annealing at each temperature in increasing steps. Blue: amorphous, Green: surface crystals, Orange: bulk crystalline. Yellow represents an intermediate structure in which the surface crystalline morphology has not been fully broken by the emergence of bulk crystallites. The labelled points (E1-H7) indicate the conditions corresponding to the AFM images shown in subsequent figures.

Fig.3-b shows the crystal stability diagram of Copolymer 9 (PET/PEN = 10/90, 5 min reacted). At this PEN-rich end of the range, the T_{cS} and T_{cB} (in agreement with DSC measurements, Table 2) are reduced from the homopolymer (PEN) as discussed in [20]. The crystalline morphology of Copolymer 9 is, however, basically similar to that of PEN (F1 to F4 in Fig.4), without the bristle-like protrusions on the crystals of thick films (F4).

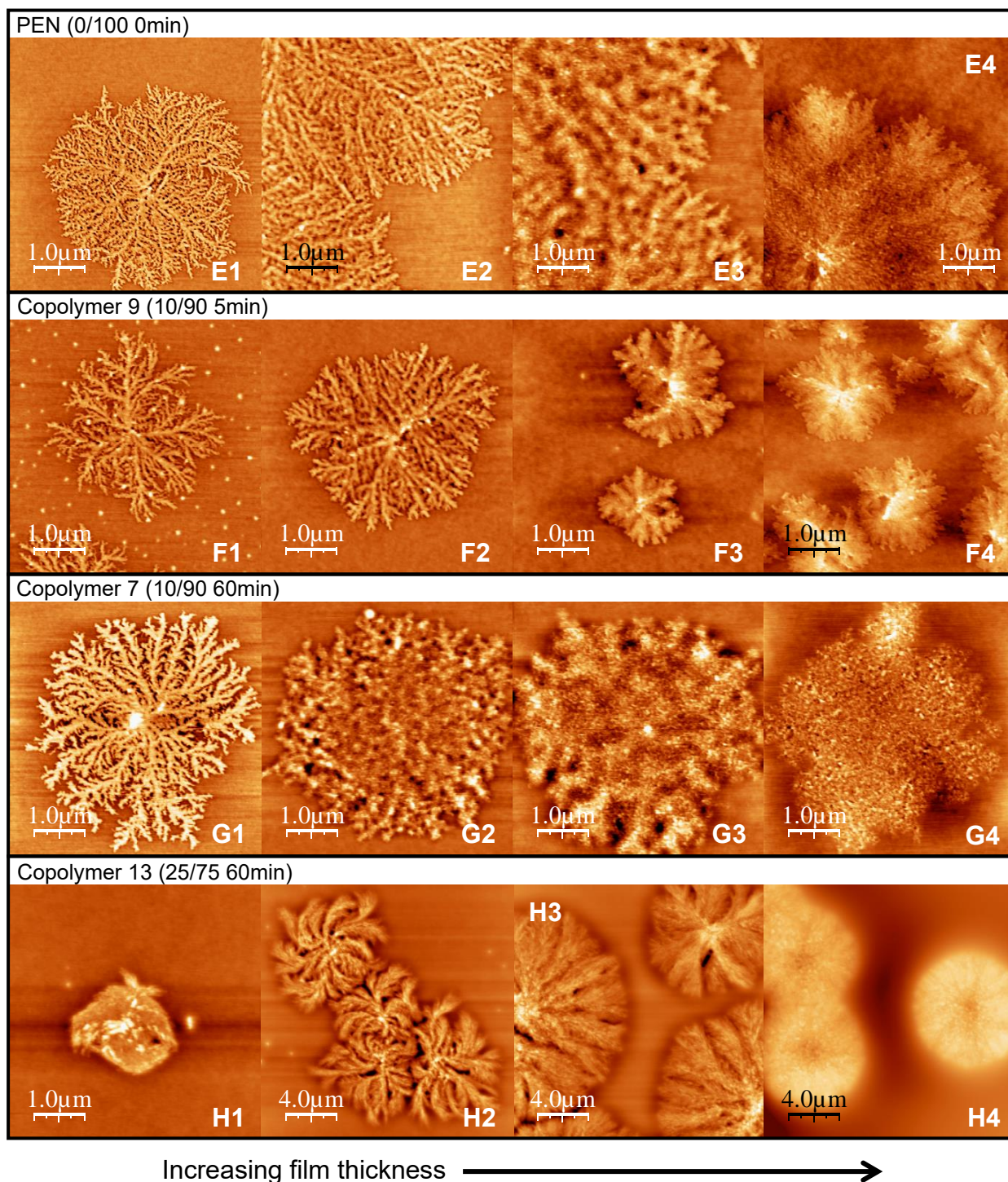


Fig.4 (Colour online) Surface crystals of PEN and PEN-rich copolymers corresponding to the crystal stability diagrams in Fig.3. Images from E1 to E4 are PEN (thicknesses 9, 27, 95 and 670 nm), F1 to F4 are Copolymer 9 (PET/PEN=10/90, 5 min reaction, thicknesses 7, 28, 71 and 580 nm), G1 to G4 are Copolymer 7 (PET/PEN=10/90, 60 min reaction, thicknesses 8, 33, 75 and 493 nm), and H1 to H4 are Copolymer 13 (PET/PEN=25/75, 60 min reaction, thicknesses 12, 30, 80 and 613 nm), respectively. Images left-to-right are from films of increasing thickness. The PEN-rich surface crystals grow out in all directions with fine branching (images E to G). There are fine bristle-like objects protrude from the surface of the crystals (E3-E4, G2-G4). In the case of Copolymer 13, the crystal morphology is not directly analogous to either PET or PEN. H1 and H2 illustrate that there are fewer branches and the lamellae radiate with curve, whereas the crystals in H4 protruded more than 200 nm from the surface with spherulitic-like morphology. The origin of the white dots in Fig F1 is unknown (most likely some contamination), but they do not appear to affect the morphology.

Copolymer 7 is a PEN-rich copolyester with the same composition as Copolymer 9, but it has undergone a longer transesterification (PET/PEN = 10/90, 60 min reacted), and therefore its sequence length L_N is shorter (20). In the surface morphology diagram of Copolymer 7 (Fig.3-c), the T_{cS} of thick films rebounds to around 115°C. Bulk crystallization was observed only for the thickest, 493 nm, film. Like Copolymer 9, Copolymer 7 exhibited a crystalline morphology (G1 to G4 in Fig.4) similar to PEN, surface crystals from G2 (32.5 nm) to G4 (493 nm) are covered with thicker bristle-like protrusions than that of PEN crystals (E3 and E4). The width of branches in the crystals of Copolymer 7 became larger than that of PEN. In particular, surface crystals on 8 nm thick film (G1) exhibited the typical morphology of diffusion-limited aggregation, which is associated with flat-on lamellar orientation [39-41].

Copolymer 13 (PET/PEN = 25/75, 60 min reacted), as expected for this shorter sequence length polymer, showed more limited range of crystallinity in the diagram (Fig.3-d). T_{cS} ascended to 135°C (20°C higher than PEN), whereas morphological T_{cB} totally disappeared. DSC results in Table 2 showed no exotherm for T_{cB} of Copolymer 13, which is consistent with the AFM results. Thus, it was shown that even though the bulk crystallization is seriously hindered by the poor sequence matching in Copolymer 13 ($L_N = 4.4$, $B = 0.91$), surface crystallization is still possible presumably due to the enhanced molecular mobility at the surface [35-38] which gives more opportunity for matching sequences to find one another. As the surface layer is a very small volume fraction in the bulky specimen for DSC measurement, the crystallization peaks would be too small to detect. This is thought to be similar to the case of Copolymer 10 (PET/PEN = 75/25) with increased T_{cS} and extinction of morphological T_{cB} , although Copolymer 10 gave a very small DSC exotherm. Also, the increase of T_{cS} in Copolymer 13 thin films is similar to the case of its PET-rich counterpart, Copolymer 10. Films thinner than 7.5 nm did not crystallize at all in copolymer 13, so even surface crystallization is inhibited.

Images H1 to H4 of Copolymer 13 in Fig.4 show a distinct morphology from the other PEN-rich copolymers. Spherulitic crystals appeared in the films of 613 nm thick (H4), similar to the PET-rich equivalent, Copolymer 10. As the films become thinner, the lamellae tend to increasingly curve, but do not contain the bristle-like protrusions observed for other PEN-rich surface crystals. By the thinnest films (H1) the high curvature of the lamellae result in their impingement to themselves from an early stage of the crystallization. Branches visible in H3, H2 and H1 are not PEN-like fine branches.

PET/PEN=50/50 copolymers

Fig.5a shows the surface morphology diagram of Copolymer 3 (PET/PEN = 50/50, 5 min reacted). The short reaction time ensures that the sequence lengths remain reasonably long ($L_T=29$ and $L_N=25$) and a T_{cS} was observed at 90°C, between PET and PEN. Bulk crystallization was only observed in the thickest, 436 nm, film. The representative surface crystalline morphology of Copolymer 3 is shown as images I1 to I4 in Fig.5. Just 5 minutes reaction produced finely branched surface crystals, which reflect both the morphology of PET-rich and PEN-rich systems. The primary nucleation rate of Copolymer 3 was so small that the surface crystals were able to grow up to a diameter of several μm without any impingement. Surface crystals on the films thicker than 15 nm were covered with bristle-like protrusions (I2 and I3), which is characteristic of PEN-rich copolymers. As the L_T and L_N of Copolymer 3 are very close one another, it is difficult to determine which component mainly contributes to crystal formation, and it might be an intermediate type comprising elements of both monomers.

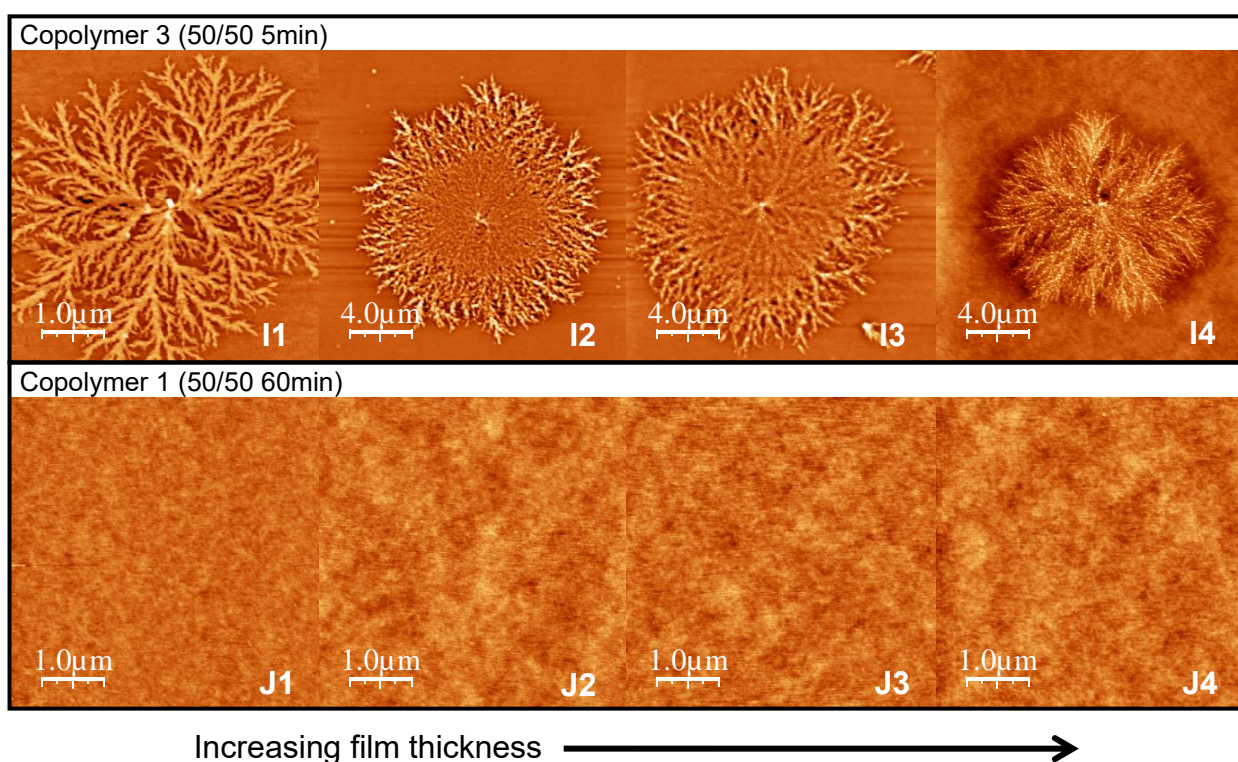
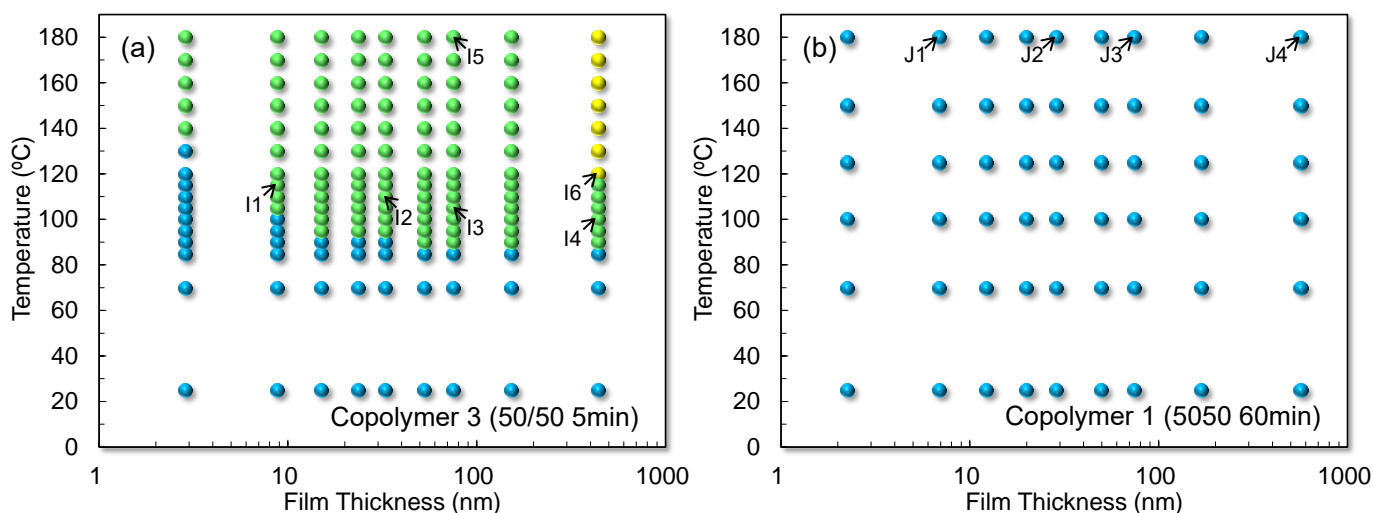


Fig.5 (Colour online) Surface morphology diagrams of the central composition of PET/PEN copolymer thin films. Surface morphology of the thin films were recorded after a 2-hour annealing at each temperature in increasing steps. Blue: amorphous and Green: surface crystals. Yellow represents an intermediate structure in which the surface crystalline morphology has not been fully broken up by the emergence of bulk crystallites. Images I1-I4 and J1-J4 indicate surface crystals of PET/PEN = 50/50 copolymers with conditions indicated on the surface morphology diagrams. Copolymer 3 (PET/PEN=50/50, 5 min reaction, thicknesses 9, 31, 75 and 436 nm) (I1-I4) produced finely branched surface crystals, which shows crystalline features intermediate between PET and PEN. Copolymer 1 (PET/PEN=50/50, 60 min reaction, thicknesses 7, 29, 72 and 570 nm) (J1-J4) gave amorphous surface even at 180°C.

After the 50/50 copolymer was reacted for 60 mins (Copolymer 1), no crystallization behaviour at all was observed for annealing temperatures up to 180 °C (Fig.5b). The L_T and L_N of Copolymer 1 were 2.1 and 1.7 respectively, which seems to be too short to crystallize, even at the mobile surface. Images J1 to J4 in Fig.5 exhibit the amorphous surface of Copolymer 1 with no crystalline

morphology even at 180 °C, suggesting that the randomness is large and the sequence length is small enough to inhibit crystalline nucleation perfectly, as supported by DSC results (Table 2). Kampert *et al.* [42] demonstrated that as the transesterification progressed, PET/PEN = 50/50 blends changed to non-crystallizable random copolymer after 25 min reaction at 285°C, which is a rather mild reaction condition compared to this work. Also, PET/PEN = 50/50 [8] and PEN/PPT = 50/50 [11] systems completely lost its crystallizability after sufficient reaction period, indicating the formation of random copolyesters.

The observations of PET/PEN copolymers suggest that as the transesterification reaction progresses, crystallizability becomes inhibited due to the shortened sequence length and increased randomness, and at some point, the resulting copolymer entirely loses its ability to crystallize. The more mobile free-surface is, however, able to crystallize more readily than the bulk even for shorter sequence lengths, suggesting a kinetic limitation to crystallization of the more random copolymers. In this study, the necessary minimum sequence length for surface crystallization would be roughly estimated between 2.1 and 4.4 for at least one component, whereas randomness (B) is not critically influential. On the other hand, the shortest sequence length for bulk crystallization is thought to be between 4.4 and 5.1 [20]. According to the data reported by Jun *et al.* [7], the critical sequence length necessary for bulk crystallization of PET/PEN copolymers is thought to be ca. 4, which is consistent with this study.

3-4. Surface morphology of highly random copolymers

In general, therefore we observe that surface crystallization occurs at lower annealing temperatures and this morphology is overtaken at higher annealing temperatures if bulk crystallization can occur. However for highly random copolymers the surface crystalline morphology appears to be more resilient.

Morphology changes once bulk crystallization begins

The surface morphology of the copolymers with high randomness and short sequence length at temperatures substantially above T_{cS} are presented in Fig.6. Image I5 (Copolymer 3 (50/50, 5min), 74.8 nm - 180°C) showed surface crystals with clear grain boundaries: no bulk crystalline morphology was observed from the surface. The anneal was well above the T_{cB} as measured by DSC (120°C), and at a film thickness of 74.8nm one might expect enough bulk material to allow crystallization, as is observed for compositions closer to the homopolymers, so we expect that some bulk crystallization is occurring under the surface. This observation implies that for the 74.8 nm thick film, the surface crystals are robust enough not to be overcome by bulk crystals emerging beneath the surface crystalline layer, even at 60°C above the T_{cB} . In contrast, once the film thickness is as great as 436 nm in the same polymer (I6), there is some change in morphology (bright dots in image I6) at 120°C, the T_{cB} as measured by DSC: a suggestion that the crystallization in the bulk region of the film is influencing the morphology observed at the surface, because of the greater thickness of the bulk layer and hence greater effect on roughness, as previously reported [18, 24]. These indications of the onset of bulk crystallization are observed particularly in the intergranular regions of the preceding surface crystallization. Similar behaviour was observed in the case of Copolymer 7 (G5 and G6). At greater film thickness, Copolymer 7 apparently developed bulk crystals which can be seen at the grain boundaries of the surface crystals, as indicated in image G6.

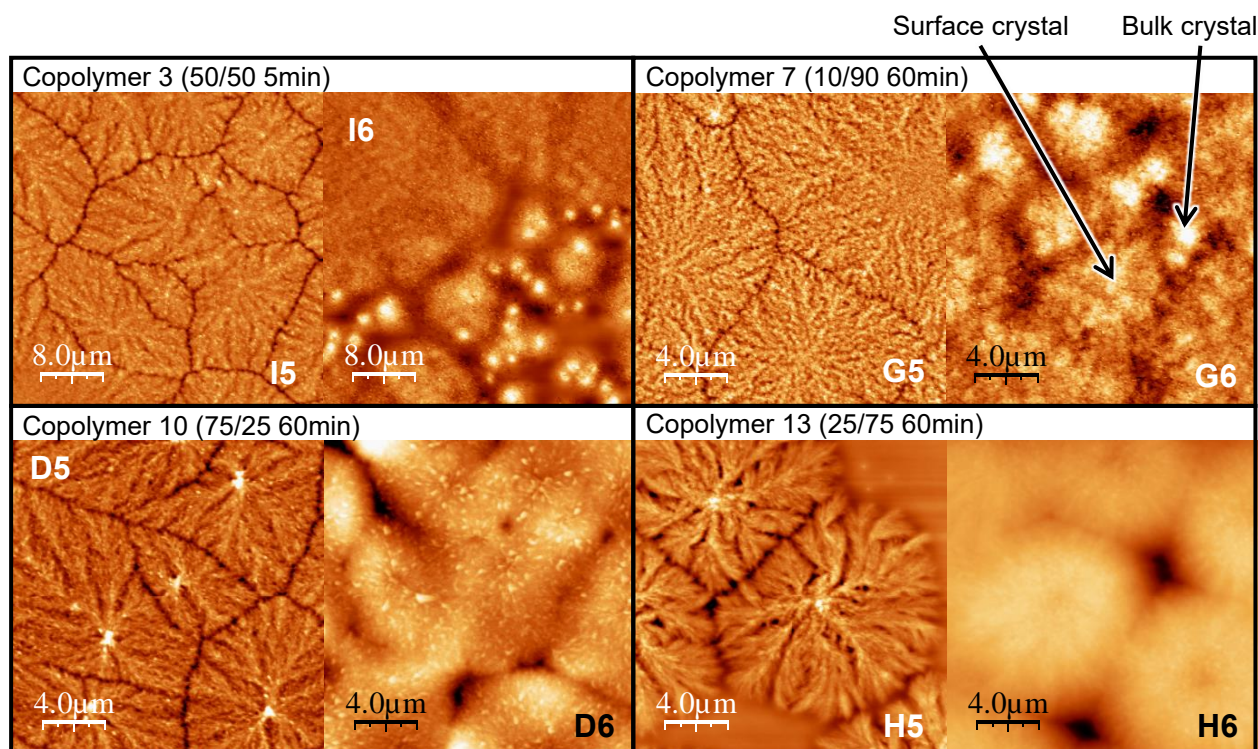


Fig.6 (Colour online) Surface morphologies of copolymers having high degree of randomness and short sequence length annealed at high temperatures. I5: Copolymer 3 (PET/PEN=50/50, 5 min reaction, 75 nm, annealed up to 180°C), I6: Copolymer 3 (PET/PEN=50/50, 5 min reaction, 436 nm, annealed up to 120°C), G5: Copolymer 7 (PET/PEN=10/90, 60 min reaction, 53.5 nm, annealed up to 190°C), G6: Copolymer 7 (PET/PEN=10/90, 60 min reaction, 493 nm, annealed up to 135°C), D5: Copolymer 10 (PET/PEN=75/25, 60 min reaction, 50 nm, annealed up to 180°C), D6: Copolymer 10 (PET/PEN=75/25, 60 min reaction, 477 nm, annealed up to 180°C), H5: Copolymer 13 (PET/PEN=25/75, 60 min reaction, 54 nm, annealed up to 190°C), H6: Copolymer 13 (PET/PEN=25/75, 60 min reaction, 613 nm, annealed up to 190°C).

The emergence of bulk crystalline morphology is thought to depend on a balance between thickness of the surface layer and thickness of the bulk layer. Crystallization in the bulk layer will reorder the material causing undulations at the surface that can obscure the previously formed surface crystals from AFM imaging. The greater the thickness of the bulk layer, the greater this disruption will be, but conversely, the thicker the surface crystalline layer, the more robust it will be against being disrupted by underlying crystallization events. If the thickness of the surface crystalline layer is increased in Copolymer 3 and 7, the tendency described above will become stronger than that of homopolymers. This speculation is supported by the measurement of depth of crevasses at the grain boundaries (Fig.7-a and Fig.7-b) that is thought to be related with the thickness of the surface layer. The details will be described in the next section. These observations also lend weight to the hypothesis that the surface crystals remain after the onset of bulk crystallization and are just obscured in the micrographs, rather than the chains in the surface crystals re-ordering to become part of bulk crystalline lamellae in an Ostwald-ripening-like process.

The 75/25 and 25/75 copolymers 10 and 13 showed no bulk crystalline morphology in this study. The surface crystals on thin films of Copolymer 10 and 13 (D5 and H5, 50 and 54 nm thick) still remained at 180 and 190°C. Even the thick films of these copolymers (D6 and H6, 477 and 613 nm thick) sustained the original spherulitic crystalline morphology even at 180 and 190°C.

Although D6 and H6 are in some ways reminiscent of bulk crystals, they are the crystalline morphologies firstly generated from the amorphous surface at low temperatures, and stepwise increase in temperature showed no further crystallization event to renew the surface morphology.

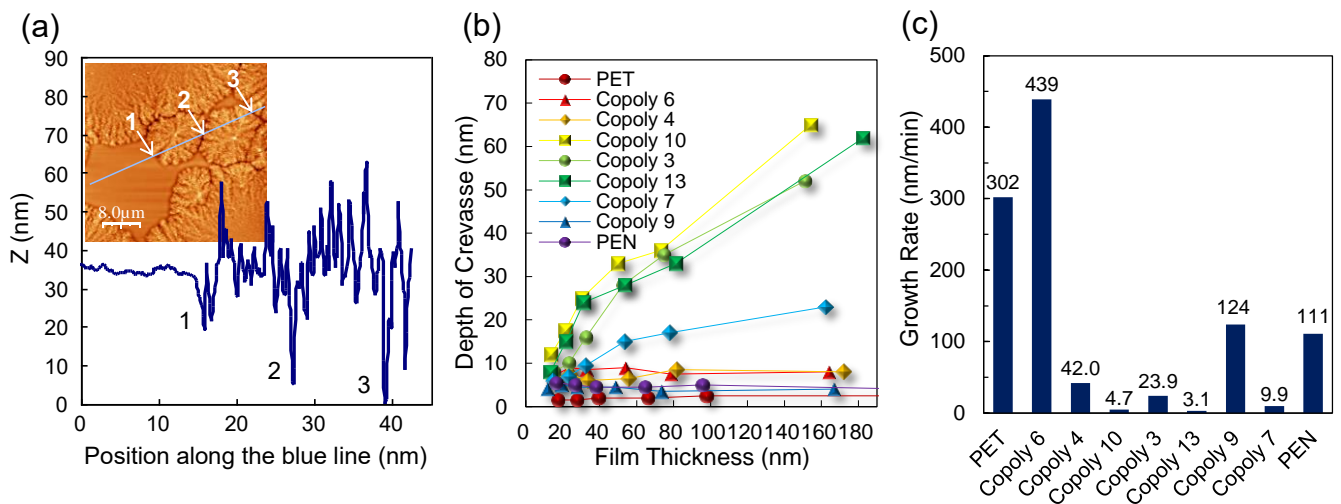


Fig.7 (Colour online) (a) An example for the measurement of depth of crevasse on a surface crystal of Copolymer 3 (PET/PEN=50/50, 5 min reaction, film thickness 74.8 nm, 130 °C). (b) Depth of crevasse of the surface crystals, showing that Copolymer 10 (PET/PEN=75/25, 60 min reaction), 13 (PET/PEN=25/75, 60 min reaction), 3, and 7 (PET/PEN=10/90, 60 min reaction) have increasing depth of crevasse depending on the film thickness, whereas Copolymer 6 (PET/PEN=90/10, 5 min reaction), 4 (PET/PEN=90/10, 60 min reaction), 9 (PET/PEN=10/90, 5 min reaction), and homopolymers have a constant value less than ca. 10 nm. (c) Surface crystal growth rate of the copolymers and homopolymers of 100 nm thick films. There are large difference in the growth rate between highly reacted copolymers and slightly reacted copolymers + homopolymers.

Thickness of PET/PEN copolymer surface crystals

Fig.7-a is an example measurement of the topographic line profile of the surface crystals of Copolymer 3 (74.8 nm thick film, 130°C). The profile shows the depths of crevasses at the grain boundaries are very large, e.g. the height gap between the bottom of a crevasse and amorphous surface level is measured to be as much as 35 nm. Likewise, the depth of crevasses of all the other copolymers and homopolymers were measured and summarised in Fig.7-b. This suggests that Copolymers 10, 13, and 3 have increasing depth of crevasses with the film thickness, whereas Copolymers 6, 4, 9, and homopolymers show a certain, smaller, constant value less than ca. 10 nm. We caution that, because of the effect of the width of the AFM tip, if the *width* of the crevasses increased, this could make the apparent depth seem greater. On the basis of the measurement of the depth of crevasses, the thicknesses of the surface crystals of Copolymers 10, 13, and 3 are estimated to be much greater than the other copolymers and homopolymers. These measured thickness of crevasses, which are thought to represent the thickness of surface crystals, are consistent with the surface and bulk crystallization behaviour reported here. For edge-on crystals the thickness of the crystalline surface layer is not the same as the lamellar thickness which, on the basis of SAXS results, Lu *et al.* [14] and Patchek *et al.* [43] reported is almost constant irrespective of the composition. (The SAXS data show that the long period of PET/PEN copolymers enlarges in the mid-range of the composition, but this can be due to the greater amount of 'rejected' inter-lamellar amorphous material in the mid-range of PET/PEN composition, which brings the greater gap between crystalline lamellae.) The apparently thicker surface crystal layers

could result from a slower crystal growth, giving more time for chains to be incorporated into the crystals, and hence allowing slightly less mobile chains further from the surface, (or material immediately next to the growing crystal which has been newly exposed to the surface), to be included in the crystal growth.

The greater crevasse depths are, broadly, associated with the more slowly growing crystals – growth rate shows a much stronger correlation to crevasse depth than composition, randomness, or block length. The linear growth rate of the surface crystals annealed above T_{cS} was obtained for 100 nm thick films as shown in Fig.7-c. There are significant differences of the growth rate in between highly reacted copolymers (Copolymer 10, 13, and 7), and slightly reacted copolymers (Copolymer 6 and 9) and homopolymers (PET and PEN). Copolymers 3 and 4 show intermediate growth rate. This is as we might expect: those polymers with long blocks of one monomer type will find matching blocks of monomer more quickly and the growth rate will be greater. All the growth rates were measured at temperatures between T_{gB} and T_{cB} (i.e. at a temperature at which we expect only the observed surface crystallization).

Thus, as the crystallization becomes less probable as the sequence length shortens, the growth rate slows. For faster growth rates the crystal development occurs only within a very near-surface region which contains highly mobile material. When the crystal growth is slow, less mobile material from slightly deeper into the film can be incorporated, and also there is more time for chains to migrate, allowing for greater protrusion of crystals from the surface and deeper trenches between.

Based on these discussions, it is possible to deduce that Copolymers 3, 7, 10, and 13 might have thicker crystalline layers at the surface than those of PET and PEN, which seal over any appearance of the bulk crystalline morphology at high temperatures. As the DSC results showed that Copolymers 3, 7 and 10 are still able to bulk-crystallize, the bulk layer beneath the crystallized surface layer is thought to produce bulk crystallites at temperatures higher than T_{cB} , but these underlying bulk crystallites are not observable with the AFM imaging.

3-5. Lamellar curvature of the surface crystals

PET/PEN copolymers with a significant major component are thought to preferentially crystallize with rejection of any heterogeneous minor component into the interlamellar amorphous, although we might expect some contamination of minor component into major component. This ‘contamination’ of the crystal structure or the rejection of material at the growth front is expected to be reflected in the crystalline morphology.

The crystalline morphology of copolymers such as PET/PEI [44], ethylene/octene [45], and random polypropylene [46] exhibit loosely organized crystals with vague boundaries. In the case of thiophene/selenophene copolymer [47], as the molecular sequence changes from blocky to random, the crystalline outline apparently vanished. This blurring of the boundary of the crystals may well be associated with constrained material rejected from the growth front of the crystal. This report is clearly different from the case of PET/PEN copolymers in this study, which exhibit distinct outlines at the crystalline boundary and detailed lamellar features against the amorphous surface even in the case of highly reacted copolymers. This suggests that the PET/PEN copolymers in this study have co-crystallized morphologies without large-scale rejection of a heterogeneous minor component into the amorphous but rather the minor component is included into the crystalline phase. (There would be small-scale rejection take place rejecting non-sequence

matched materials into the interlamellar amorphous or lamellar fold face, but a large-scale rejection resembling phase separation does not occur.)

Images D7 and H7 in Fig.8 show examples of morphologies with highly curved lamellae winding both clockwise and anticlockwise. Copolymer 10 (D7: PET/PEN=75/25, 60 min reaction) and Copolymer 13 (H7: PET/PEN=25/75, 60 min reaction), which both have high randomness and short sequence length, tend to exhibit the deformed lamellar morphology in films thinner than about 50nm. These morphologies are reminiscent of the study on ultrathin films of poly(ϵ -caprolactone)/poly(vinyl chloride) (PCL/PVC) [48], and poly(l-lactide)/poly(d-lactide) (PLLA/PDLA) [39, 49, 50] blends, which produced lamellar curvatures of both handedness. PEN was observed to show curved crystals in very thin films [24] in which crystallization is highly constrained, but otherwise such morphology was only observed in the highly random copolymers in the PET/PEN system.

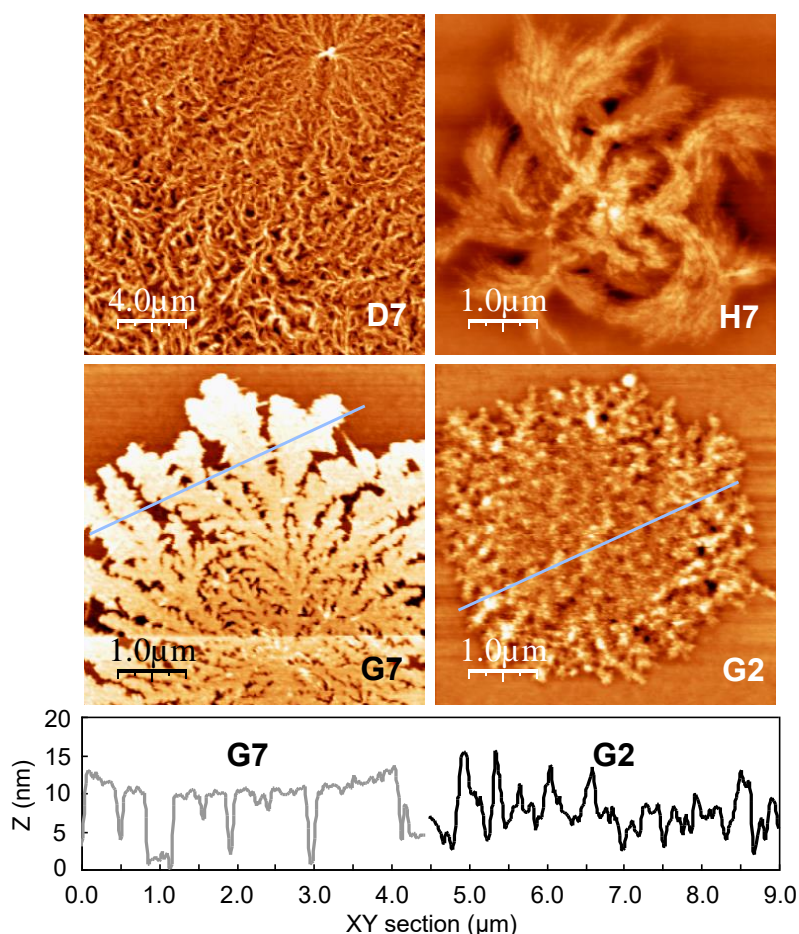


Fig.8 (Colour online) (D7 and H7) Copolymers having high degree of randomness and short sequence length tend to show a winding and diverging morphology with plenty of arbitrary minor structural deformation, which is clearly observed particularly in thin films at high temperature range. D7: Copolymer 10 (PET/PEN=75/25, 60 min reaction, 21.5 nm, annealed up to 180°C), H7: Copolymer 13 (PET/PEN=25/75, 60 min reaction, 21.7 nm, annealed up to 180°C). (G7 and G2) Flat-on and edge-on lamellae of Copolymer 7 (PET/PEN=10/90, 60 min reaction). Lines in images G7 and G2 correspond to the XY cross section of the surface crystals below. G7 shows morphology of the diffusion limited aggregation with a constant lamellar thickness implying it is a flat-on single crystal, whereas G2 shows many irregular ridges implying it is a complex entity of lamellae mainly consist of edge-on crystal. G7: 8.4 nm, annealed up to 190°C, G2: 32.5 nm, annealed up to 125°C.

The curvature of the lamellar growth of Copolymer 10 and 13 might be due to accumulated stress on the lamellar surface caused by altered unit cell parameters [7, 14, 43] in crystals where there is significant co-crystallization because of short sequence lengths (75/25 and 25/75 composition) but nevertheless an imbalance of sequence lengths giving rise to stress where the minor components are incorporated. By contrast, the short sequence length, balanced composition films (Copolymer 3) do not show such curvature. Turning of the growth direction can be attained at arbitrary points where stress on the lamellar surface becomes large, in a similar manner to the helical lamellar twisting in the spherulites of polyesters [51,52]. Electron diffraction measurement of PCL/PVC blend thin films indicated that the c axis is tilted against the lamellar fold surface while a and b axes are parallel to the substrate, suggesting that the chain tilting produces stress on the lamellar surface giving the curvature in the growth direction [48]. In the case of PLLA/PDLA blend system [39], the curvature of the crystal growth is attributed to the unbalanced mechanical stress caused by the unequally supplied PLLA and PDLA at the growth front. It was demonstrated that the growth direction of the PLLA/PDLA crystal curvature depends on crystallization temperature, film thickness, and composition of the blends, that is not fully understood presently [39].

3-6. Flat-on and edge-on lamellae of the surface crystals

Based on selected area electron diffraction analysis, it has been reported that some polymers such as isotactic poly(1-butene) [53], isotactic polystyrene [54], and polyamide 6 [55] produce flat-on single crystals when the film thickness is very small. In this study, it was observed that there is a particular film thickness range less than around 10-15 nm, in which surface crystals exhibit broad lamellae in the plane consistent with flat-on lamellar morphology. Images G7 and G2 in Fig.8 show line profiles of the topographic cross sections of surface crystals of Copolymer 7 (PET/PEN=10/90, 60 min reaction). The 8.4 nm thick film (G7) exhibits a constant lamellar height suggesting it is a flat-on crystal with the fold surface parallel to the substrate. As the annealing temperature increased stepwise, and the growth front moved away from the nucleus of the dendritic crystallite, the lamellar width and thickness dilated gradually, presumably reflecting the easier migration of molecules to the growth front. The morphological outlines of the surface crystal in G7 clearly exhibited seaweed-like diffusion-limited aggregation [39, 40, 41], which is characteristic of flat-on lamellar crystals.

On the other hand, if film thickness becomes sufficiently large, it has been reported that some polymers tend to produce edge-on lamellar orientation [55, 56, 57]. The profile of the lamellae of Copolymer 7 generated on 32.5 nm thick film (G2) does not show a constant height but many irregular protruded ridges suggesting it is stacks of edge-on lamellae. In this study, all the crystals of homopolymers and copolymers generated on films thicker than around 15-20 nm showed edge-on stacked lamellae.

On the basis of the morphological consideration, it is thought that PET/PEN copolymer surface crystals basically consist of lamellar crystals whose orientation is influenced by film thickness. Ma *et al.* [58] reported a possible explanation for the switching of the lamellar orientation. According to their Monte Carlo simulation, slippery substrates induce surface assisted nucleation resulting in edge-on lamellae, whereas sticky substrates induce self-seeded nucleation resulting in flat-on lamellae. The observed results in this study imply that the interface between bulk and surface layers is slippery because films thicker than ca. 10 nm produce edge-on crystals, whereas the surface of the silicon substrate seems sticky because films thinner than ca. 10 nm preferentially

induces flat-on orientation. The substrate surface is anticipated to have affinity with polyester molecules, which can be observed in the results of crystallization behaviour of ultra-thin films (thinner than 10 nm) in their increased T_{cs} and morphology (Fig.1, 3, and 5). In contrast, the interface between the surface and bulk layer is anticipated to be slippery because this is the boundary where mobile rubbery chains creep on the less mobile bulk layer towards the crystallizing growth front. This is consistent with our previous study on calculation of average thickness of the surface layer in PET films of 13.6 nm [18]. For instance, judging from the morphological features and thickness of the film, the AFM images in Fig.5 show that I1 might be flat-on, whereas image I2, I3, and I4 seems to be edge-on orientation.

The lamellar orientation of the surface crystals of PET/PEN copolymers have not been examined by a diffraction method such as selected area electron diffraction or grazing incidence x-ray diffraction, hence it is necessary to confirm the lamellar orientation directly for more detailed discussions in the future.

3-7. Spherulitic surface crystals in highly reacted copolymers

In the case of Copolymer 10, 13, 3 and 7, the thickness of the surface crystal is thought to increase as shown in Fig.7-b, allowing more growth of the crystals into the depth of the surface layer giving rise to a less constrained, more spherulitic-like morphology.

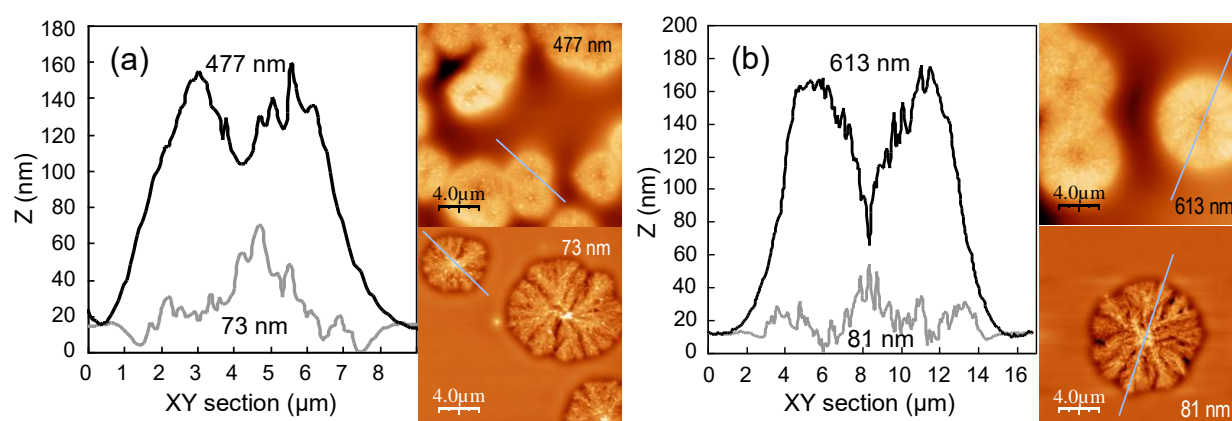


Fig.9 (Colour online) XY profiles of surface crystals of Copolymer 10 (image (a), PET/PEN=75/25, 60 min reaction) and Copolymer 13 (image (b), PET/PEN=25/75, 60 min reaction). Lines in the AFM images correspond to the XY cross section of surface crystals for each film thickness. Thin films (73 and 81 nm) have a protruded crystal nucleus, whereas thick films (477 and 613 nm) develop a hollow in the centre.

Fig.9 shows line profiles of surface crystals of Copolymer 10 and 13. When the film thickness of Copolymer 10 is smaller than ca. 200 nm, e.g. 73 nm thick in Fig.9-a, it produced surface crystals whose central nucleus is the highest point, whereas thick films such as 477 nm developed spherulitic crystals protruding about 130 nm height from the amorphous film surface with a central hollow of about 50 nm depth (Fig.9-a). As shown in Fig.9, the height of the nuclei on 73 nm and 477 nm thick films of Copolymer 10 are not very different from one another. If the primary nucleation produces nuclei with a constant height from the amorphous surface in both 73 and 477 nm thick films, and the subsequent secondary crystal growth produces surrounding crystalline entity whose thickness depends on the thickness of the surface layer of each film, a developed crystal on 73 nm thick film will have a protruded central nucleus, whereas 477 nm thick film develops an apparent hollow in the centre of a spherulitic thick crystal. A similar observation is made for

Copolymer 13 (Fig.9-b). The unique surface crystals with a protrusion or a hollow in the centre, developed on the films of Copolymer 10 and 13, resemble the surface crystals of poly(L-lactide) [59].

Obviously, the protrusion of the crystal nuclei becomes smaller if the film thickness becomes smaller than around 40 nm. Thus, the crystal nuclei with a constant height discussed above is not observed in the very thin films.

4. Conclusions

1. A full, systematic study of a series of PET/PEN copolymer thin films with various composition, sequence length and randomness, and thickness showed diversified crystallizability and unique morphologies. The morphology of the surface crystals is basically categorised into PET-like (Copolymers 6, 4, and 10), PEN-like (Copolymers 9, 7, and 13), and the intermediate of the two types (Copolymer 3).
2. SFM force-distance curve measurements detected the T_{gS} of the copolymers up to several tens of degrees below their T_{gB} obtained by DSC. The difference between T_{gS} and T_{gB} became small in the shorter sequence length Copolymers 10, 13, 3, and 7, that might give rise to the observed apparent thickening of the surface layer. This apparent thickening was evidenced by increased crevice depth at the impingement lines between crystallites, and also the more spherulitic-like morphologies that moved from having a protruding central nucleation point for films with thinner surface layer to a hollow at the central nucleation point for films with thicker surface layer.
3. The morphological T_{cS} of the thicker films was found to be several degrees lower than the T_{cB} by DSC, with the onset temperature of crystallization raised for the thinnest films to a degree that depended on copolymer composition and randomness. Surface crystals in films thinner than ca.100 nm showed significantly increased thermal stability. The surface morphologies showed no bulk crystalline morphologies in all the thicknesses of Copolymers 10 (75/25, 60min) and 13 (25/75, 60min), and in films less than 400 nm thick of Copolymers 3 (50/50, 5min) and 7 (10/90, 60min) films, which is either because no bulk crystallization is occurring (no T_{cB} by DSC for copolymer 13, and for very thin films in other polymers all bulk crystallization may be inhibited) or because, for some compositions, thick surface crystals conceal the appearance of the bulk crystalline morphology.
4. In most conditions the crystal lamellae show distinct edges, contrary to what has been observed in crystals in the literature that reject a lot of material at the growth front, lending support to the idea that co-crystallization is occurring in this, confined, surface crystallinity, and this is further supported by the observation that thin films (less than ca. 22 nm) of Copolymers 10 and 13 produce surface crystals with a curved lamellae which is thought to be caused by changes in the unit cell parameters due to their poor sequence matching.

5. References

1. Evans, R. D., Mighton, H. R. and Flory, P. J. *J. Chem. Phys.* **1947**, *15*, 685–685.
2. Wunderlich, B. *J. Chem. Phys.* **1958**, *29*, 1395–1404.
3. Briber, R. M. and Thomas, E. L. *Polymer* **1985**, *26*, 8–16.
4. Park, S. S., Chae, S. H. and Im, S. S. *J. Polym. Sci. Part A: Polym. Chem. Ed.* **1998**, *36*, 147–156.
5. Jin, J., Du, J., Xia, Q., Liang, Y. and Han, C. C. *Macromolecules* **2010**, *43*, 10554–10559.
6. Li, W., Kong, X., Zhou, E. and Ma, D. *Polymer* **2005**, *46*, 11655–11663.
7. Jun, H. W., Chae, S. H., Park, S. S., Myung, H. S. and Im, S. S. *Polymer* **1999**, *40*, 1473–1480.
8. Wu, G. and Cuculo, J. A. *Polymer* **1999**, *40*, 1011–1018.
9. Hu, Y. S., Hiltner, A. and Baer, E. *J. Appl. Polym. Sci.* **2005**, *98*, 1629–1642.
10. Krutphun, P. and Supaphol, P. *Eur. Polym. J.* **2005**, *41*, 1561–1568.
11. Woo, E. M., Hou, S. -S., Huang, D. -H. and Lee, L. -T. *Polymer* **2005**, *46*, 7425–7435.
12. Windle, A. H., Viney, C., Golombok, R., Donald, A. M. and Mitchell, G. R. *Faraday Discuss.* **1985**, *79*, 55–72.
13. Lu, X. and Windle, A. H. *Polymer* **1996**, *37*, 2027–2038.
14. Lu, X. and Windle, A. H. *Polymer* **1995**, *36*, 451–459.
15. Welsh, G. E. and Windle, A. H. *Polymer* **2001**, *42*, 5727–5735.
16. Hanna, S., Romo-Uribe, A. and Windle, A. H. *Nature* **1993**, *366*, 546–549.
17. Gutierrez, G. A., Chivers, R. A., Blackwell, J., Stamatoff, J. B. and Yoon, H. *Polymer* **1983**, *24*, 937–942.
18. Shinotsuka, K., Bliznyuk, V. N. and Assender, H. E. *Polymer* **2012**, *53*, 5554–5559.
19. Xu, J., Li, Y., Wu, X., Zuo, B., Wang, X., Zhang, W. and Tsui, O. K. C. *Macromolecules* **2018**, *51*, 3423–3432.
20. Shinotsuka, K., Assender, H. E. and Claridge, T. D. W. *Journal of Applied Polymer Science* **2018**, *135*, 46515.
21. Yoon, K. H., Lee, S. C., Park, I. H., Lee, H. M., Park, O. O. and Son, T. W. *Polymer* **1997**, *38*, 6079–6081.
22. Brandrup, J.; Immergut, E. H. *Polymer Handbook Third Ed.* **1989**, Wiley-Interscience.
23. Yamadera, R. and Murano, M. *J. Polym. Sci., Part A-1* **1967**, *5*, 2259–2268.
24. Shinotsuka, K. and Assender, H. E. *J. Appl. Polym. Sci.* **2016**, *133*, 44269.
25. Bliznyuk, V. N., Assender, H. E. and Briggs, G. A. D. *Macromolecules* **2002**, *35*, 6613–6622.
26. Marti, O., Stifter, T., Waschipsky, H., Quintus, M. and Hild, S. *Colloids Surf. A: Physicochemical and Engineering Aspects* **1999**, *154*, 65–73.
27. Tsui, O.K.C., Wang, W.P., Ho, J.Y.L., Ng, T.K. and Xiao, X. *Macromolecules* **2000**, *33*, 4198–4204.
28. Kaliappan, S.K. and Capella, B. *Polymer* **2005**, *46*, 11416–11423.
29. Shi, Y. and Jabarin, S. A. *J. Appl. Polym. Sci.* **2001**, *80*, 2422–2436.
30. Tharmapuram, S. R. and Jabarin, S. A. *Adv. Polym. Technol.* **2003**, *22*, 137–146.
31. Tao, W., Wei, W., Yu, C., Ren, W. and Qiaoling, L. *J. Appl. Polym. Sci.* **2013**, *130*, 673–679.
32. Geyer, B., Röhner, S., Lorenz, G. and Kandelbauer, A. *J. Appl. Polym. Sci.* **2014**, *131*, 40731.
33. Khonakdar, H. A., Golriz, M., Jafari, S. -H. and Wagenknecht, U. *Macromol. Mater. Eng.* **2009**, *294*, 272–280.

34. Röhner, S., Geyer, B., Gad'on, S., Kandelbauer, A., Chassé, T. and Lorenz, G. *J. Appl. Polym. Sci.* **2015**, *132*, 41997.
35. Keddie, J. L., Jones, R. A. L. and Cory, R. A. *Europhys. Lett.* **1994**, *27*, 59–64.
36. Pratt, F. L., Lancaster, T., Brooks, M. L., Blundell, S. J., Prokscha, T., Morenzoni, E., Suter, A., Luetkens, H., Khasanov, R., Shinotsuka, K. and Assender, H. E. *Phys. Rev. B* **2005**, *72*, 121401R.
37. Gao, S., Koh, Y. P. and Simon, S. L. *Calorimetric Macromolecules* **2013**, *46*, 562–570.
38. Chai, Y., Salez, T., McGraw, J. D., Benzaquen, M., Dalnoki-Veress, K., Raphaël, E. and Forrest, J. A. *Science* **2014**, *343*, 994–999.
39. Wang, X. and Prud'homme, R. E. *Macromolecules* **2014**, *47*, 668–676.
40. Zhang, G., Jin, L., Zheng, P., Shi, A. -C. and Wang, W. *Polymer* **2010**, *51*, 554–562.
41. Yu, C., Xie, Q., Bao, Y., Shan, G. and Pan, P. *Crystals* **2017**, *7*, 147.
42. Kampert, W. G. and Sauer, B. B. *Polymer* **2001**, *42*, 8703–8714.
43. Patcheak, T. D. and Jabarin, S. A. *Polymer* **2001**, *42*, 8975–8985.
44. Hu, Y. S., Hiltner, A. and Baer, E. *J. Appl. Polym. Sci.* **2005**, *98*, 1629–1642.
45. Khariwala, D. U., Taha, A., Chum, S. P., Hiltner, A. and Baer, E. *Polymer* **2008**, *49*, 1365–1375.
46. Luo, F., Zhu, Y., Wang, K., Deng, H., Chen, F., Zhang, Q. and Fu, Q. *Polymer* **2012**, *53*, 4861–4870.
47. Palermo, E. F. and McNeil, A. J. *Macromolecules* **2012**, *45*, 5948–5955.
48. Mamun, A., Mareau, V. H., Chen, J. and Prud'homme, R. E. *Polymer* **2014**, *55*, 2179–2187.
49. Maillard, D. and Prud'homme, R. E. *Macromolecules* **2010**, *43*, 4006–4010.
50. Marubayashi, H., Nobuoka, T., Iwamoto, S., Takemura, A. and Iwata, T. *ACS Macro Lett.* **2013**, *2*, 355–360.
51. Lotz, B. and Cheng, S. Z. D. *Polymer* **2005**, *46*, 577–610.
52. Rosenthal, M., Burghammer, M., Bar, G., Samulski, E. T. and Ivanov, D. A. *Macromolecules* **2014**, *47*, 8295–8304.
53. Zhang, B., Yang, D. and Yan, S. *J. Polym. Sci., Part B: Polym. Phys.* **2002**, *40*, 2641–2645.
54. Taguchi, K., Miyamoto, Y., Miyaji, H. and Izumi, K. *Macromolecules* **2003**, *36*, 5208–5213.
55. Zhong, L. -W., Ren, X. -K., Yang, S., Chen, E. -Q., Sun, C. -X., Stroeks, A. and Yang, T. -Y. *Polymer* **2014**, *55*, 4332–4340.
56. Kikkawa, Y., Abe, H., Fujita, M., Iwata, T., Inoue, Y. and Doi, Y. *Macromol. Chem. Phys.* **2003**, *204*, 1822–1831.
57. Schönherr, H. and Frank, C. W. *Macromolecules* **2003**, *36*, 1188–1198.
58. Ma, Y., Hu, W. and Reiter, G. *Macromolecules* **2006**, *39*, 5159–5164.
59. Yuryev, Y., Wood-Adams, P., Heuzey, M. -C., Dubois, C. and Brisson, J. *Polymer* **2008**, *49*, 2306–2320.

7. Acknowledgements

The authors express our appreciation to the financial support by Oji Paper Co., Ltd. We thank Mr. Kimihiro Ogawa in Teijin Chemical Co., Ltd. for his kind offer of PEN pellets and its instructions. We acknowledge for Prof. Timothy D. W. Claridge at the Chemistry Department in the University of Oxford for his kind collaboration on ^1H NMR analysis.